Lithuanian Journal of Physics
Vol. **64**, No. 4, pp. 244–252 (2024)
ISSN 1648-8504 eISSN 2424-3647
DOI: https://doi.org/10.3952/physics.2024.64.4.5

# OPTIMIZATION OF AlGaAs BARRIER FOR InGaAs QUANTUM WELLS EMITTING IN THE NEAR INFRARED

**A. Zelioli [a], J. Žuvelis [a, b], U. Cibulskaitė [b], A. Špokas [a, b], E. Dudutienė [a], A. Vaitkevičius [a, b], S. Stanionytė [a], B. Čechavičius [a], and R. Butkutė [a]**

[a] *State Research Institute Center for Physical Sciences and Technology, Saulėtekio 3, 10257 Vilnius, Lithuania*
[b] *Institute of Photonics and Nanotechnology, Vilnius University, Saulėtekio 3, 10257 Vilnius, Lithuania*
Email: andrea.zelioli@ftmc.lt

Received 12 November 2024; accepted 12 November 2024

The results of a study aimed at optimizing the optical properties of InGaAs quantum well structures by employing different barrier designs are presented. Single rectangular InGaAs quantum wells with approximately 21% indium and AlGaAs barriers, with different Al content 12, 20 and 30%, were theoretically modelled using the next**nano**[3] software to calculate band edges and levels in the quantum wells. A series of samples were grown using molecular beam epitaxy to clarify the influence of the Al fraction in the AlGaAs barriers on the optical properties of the quantum structures. Atomic force microscopy measurements were used to evaluate the surface roughness of the grown structures, while photoluminescence investigations provided insight into the optical quality and carrier confinement effects. The investigations revealed that the introduction of AlGaAs barriers resulted in an increased carrier confinement inside of the quantum well, but consequently resulted in the degradation of the InGaAs quantum well quality with the increase of aluminium content in the barrier. It was determined that a barrier with 12% of Al can be used to balance these effects, by providing a sufficient confinement, while retaining a satisfactory crystalline quality of the quantum structures.

**Keywords:** AIII-BV, molecular beam epitaxy, near infrared, photoluminescence, atomic force microscopy, X-ray diffraction

## 1. Introduction

Semiconductor lasers are solid state lasers that use a semiconductor gain medium, where optical amplification is achieved through stimulated emission at an interband transition. InGaAs/GaAs multi-quantum wells (MQWs) are commonly used in applications such as light-emitting diodes, near-infrared lasers, photodetectors, and photovoltaic devices, owing to their high radiation efficiency and broad spectral range [1–4]. In many applications, the lasing efficiency is one of the main characteristics of these emitters [5]. Therefore, improving efficiency in QW-based lasers involves enhancing the material quality, minimizing defects, and achieving sharp interfaces.

However, using rectangular InGaAs/GaAs MQWs as the active region in optoelectronic devices faces limitations due to the insufficient barrier height of GaAs, which is insufficient to effectively confine carriers. This limitation affects temperature stability and restricts the achievement of optimal optical gain [6, 7]. Alternative QW designs, such as step-like quantum barriers and electron blocking layers, have been shown to enhance the radiative recombination rate in electrically pumped laser diodes. These designs often incorporate compounds like AlGaAs to provide higher potential barriers, thereby suppressing carrier leakage [8].

The growth of AlGaAs and InGaAs requires different optimal substrate temperature windows. AlGaAs has been shown to have the highest quality when grown at temperatures from 600 up to 720°C, with the best results observed at the higher end of this temperature range [9–11]. When grown at temperatures below 580°C, the AlGaAs quality deteriorates significantly [12, 13].In contrast, InGaAs

is typically grown at temperatures between 450 and 540°C. At higher temperatures, In re-evaporation intensifies, reducing the incorporation of In, and increasing the segregation length of In atoms [14–17]. Additionally, interdiffusion between In and Ga atoms could result in the formation of a disordered AlInGaAs quaternary alloy at the interface between the InGaAs well layer and the AlGaAs barrier layer [18]. This random diffusion behaviour increases the roughness of heterointerfaces. Recently, incorporating ultrathin GaAs insertion layers (ISLs) of various thicknesses has been demonstrated to effectively improve the interface quality and enhance the optical properties of QWs [19–22].

This study investigates the effect of barrier composition on the light generation efficiency of various InGaAs QW structures designed for the gain region of vertical-external-cavity surface-emitting lasers (VECSELs) operating in the near-infrared (NIR) spectral range. Quantum wells of a uniform thickness and a similar indium content were modelled and grown with varying barrier compositions, employing GaAs and AlGaAs with different aluminium concentrations. Temperature- and excitation-dependent photoluminescence (PL) measurements, along with theoretical calculations, atomic force microscopy (AFM) and X-ray diffraction (XRD), were conducted to assess the influence of the different Al concentration in the barrier layers on radiative recombination efficiency.

## 2. Methods

### *2.1.Modelling*

The structures were simulated using the next**nano**[3] software, which enables full-band quantum mechanical simulations. A one-dimensional (1D) simulation along the growth direction ($z$ axis) was performed. The band structure was modelled using the 8 × 8 k·p method with the effective mass approximation [17]. Only the conduction band minimum at the Γ point was considered, while the two valence band maxima – heavy holes (hh) and light holes (lh) – were also calculated. Excitonic effects were included in the simulations, and the temperature dependence of the band gap was taken into account. Since both AlGaAs and GaAs share the same lattice constant, strain effects were not considered in the model.

Four structures were modelled, each containing a single InGaAs QW with an identical nominal thickness and indium content, but different barrier compositions. Figure 1 illustrates the schematic representations of these samples. Sample A0, shown in Fig. 1(a), has GaAs barriers, while samples A12, A20 and A30 (Figs. 1(b–d), respectively) have AlGaAs barriers with aluminum concentrations of 12, 20 and 30%, respectively. The nominal barrier thickness was 15 nm in all cases. Each structure contains a nominal indium content of 20.8% and a QW thickness of 5.7 nm. The selection of quantum wells thickness and indium content was based on previous works [23]. These allow for emission in the NIR range, particularly around 976 nm, while minimizing the formation of lattice mismatch dislocations that could limit the total emission surface of a VECSEL chip. In Fig. 2(a, b), the PL map and $\mu$PL map of a sample fabricated with the optimized In content in the QW and the barrier design are shown, respectively. By the absence of lines of reduced intensity, we can conclude that the QW layers are free from lattice mismatch dislocations.

### *2.2. Sample growth*

The samples were grown on the quarter sections of 2-inch semi-insulating GaAs wafers. Prior to the growth, the substrate was degassed at 700°C under an arsenic overpressure until a clear 2 × 4 reconstruction pattern appeared. A 150 nm GaAs buffer layer was then grown at a substrate temperature of 650°C to ensure a high degree of surface smoothness, followed by the deposition of the first barrier at the same temperature. The substrate temperature was subsequently lowered to 580°C for the growth of a single QW (SQW) and the second barrier. Temperature measurements were carried out using a thermocouple placed between the heater and the sample. Growth rates were 490 nm/h for GaAs, 621 nm/h for InGaAs, and 697, 615 and 562 nm/h for AlGaAs with 30, 20 and 12% aluminum concentrations, respectively. To prevent the oxidation of AlGaAs barriers, a 20 nm GaAs cap layer was grown atop each sample.

The growth rates of different compounds were monitored by tracking intensity oscillations from

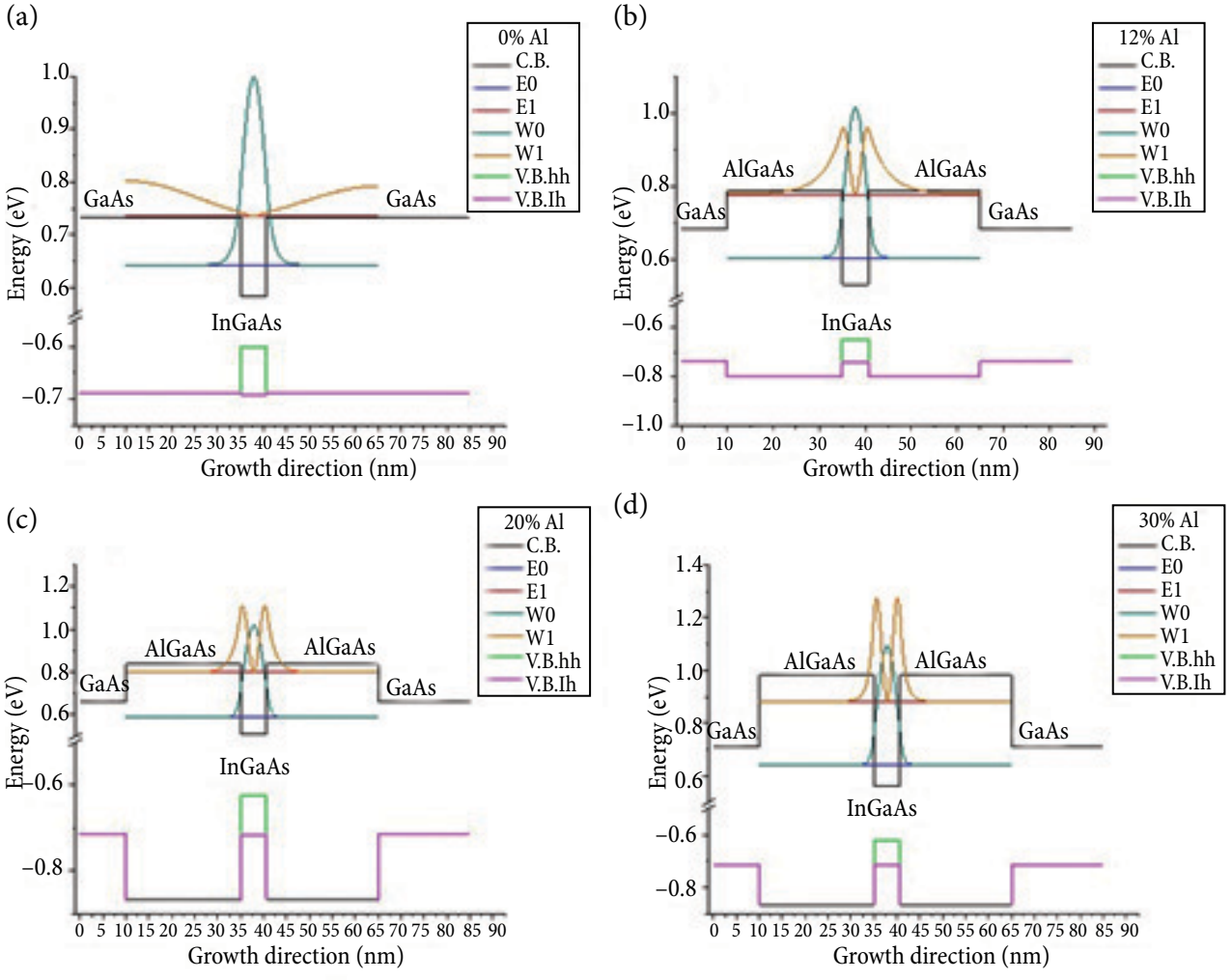


Fig. 1. Calculated band edges in the gamma point for the different structures analysed. C. B. is the conduction band edge, V. B. edges are shown for both heavy holes (hh) and light holes (lh), the electron energy level is calculated: E0 is the ground state, E1 is the first exited state, W0 and W1 are the corresponding wavefunctions. (a) InGaAs QW with GaAs barriers and one level is inside the QW. (b) InGaAs QW with AlGaAs barriers containing 12% Al and two levels are inside the QW. (c) InGaAs QW with AlGaAs barriers containing 20% Al and two levels are inside the QW. (d) InGaAs QW with AlGaAs barriers containing 30% Al and two levels are inside the QW.

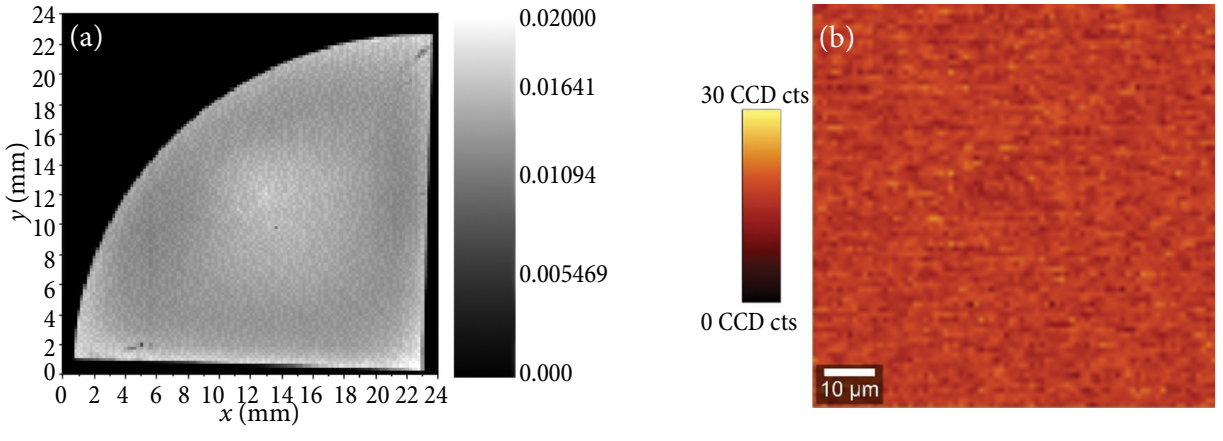


Fig. 2. Maps of the sample grown with the optimized In content in the QW and the barrier thickness in order to suppress the formation of lattice mismatch dislocations. (a) RTPL map, (b) $\mu$PL map.

*in-situ* reflection high-energy electron diffraction (RHEED). The indium and aluminum contents were controlled by adjusting the flux ratios of Ga, In and Al. The compositions were calculated using the formula

$$x\% = (1 - GR_{GaAs}/GR_{ternary}) \cdot 100\%,$$

where $x$% is the Al or In content, and GR represents the growth rate of GaAs or the ternary compounds, InGaAs or AlGaAs. Observation of the RHEED pattern during the growth provided insights into the crystalline quality of the layers through the surface reconstruction analysis.

### *2.3. Sample characterization*

Room-temperature photoluminescence (RTPL) mappings were conducted using a diode-pumped solid-state (DPSS) laser with an emission wavelength of 532 nm, delivering an intensity of approximately 5 kW/cm$^2$ and a spot size of about 50 $\mu$m on the sample. The detection system comprised a 420 nm focal length monochromator and a thermoelectrically cooled InGaAs photodetector. Scanning was facilitated by mounting the samples on motorized *xy* linear stages (8MT175-100) with a resolution of 0.31 $\mu$m, and a step size of 0.2 mm was used for the mapping.

For temperature-dependent (TD) PL measurements, the samples were mounted on a cold finger within a closed-cycle He cryostat, coupled with a temperature controller, enabling measurements across the temperature range from 3.5 to 300 K. The intensity of the 532 nm laser was reduced to 174 Wcm$^{-2}$ during the TDPL experiment.

Atomic force microscopy (AFM) and microphotoluminescence ($\mu$PL) measurements were carried out using the Witec 300S microscopy system. Continuous-wave (CW) laser excitation was provided by a diode emitting at 665 nm (*Integrated Optics*), with the laser beam focused onto the sample via a 100x objective lens with a numerical aperture of 0.9. The emitted PL signal was collected by the same objective lens and directed to an *Andor* Shamrock spectrometer, which was coupled with a thermoelectrically cooled *Andor* iDus InGaAs camera for detection. AFM measurements were performed in contact. To evaluate the roughness the root mean square height RMS (Sq) was calculated.

## 3. Results and discussion

The samples were characterized using the RTPL measurements after growth, and the corresponding spectra are presented in Fig. 3(a). Given different barrier materials, a shift in the PL emission peak was anticipated. Specifically, the introduction of aluminium into GaAs increases the bandgap and raises the QW barrier height, thereby increasing the emission energy. In the spectra of samples A30, A20 and A12, no shift is observed.

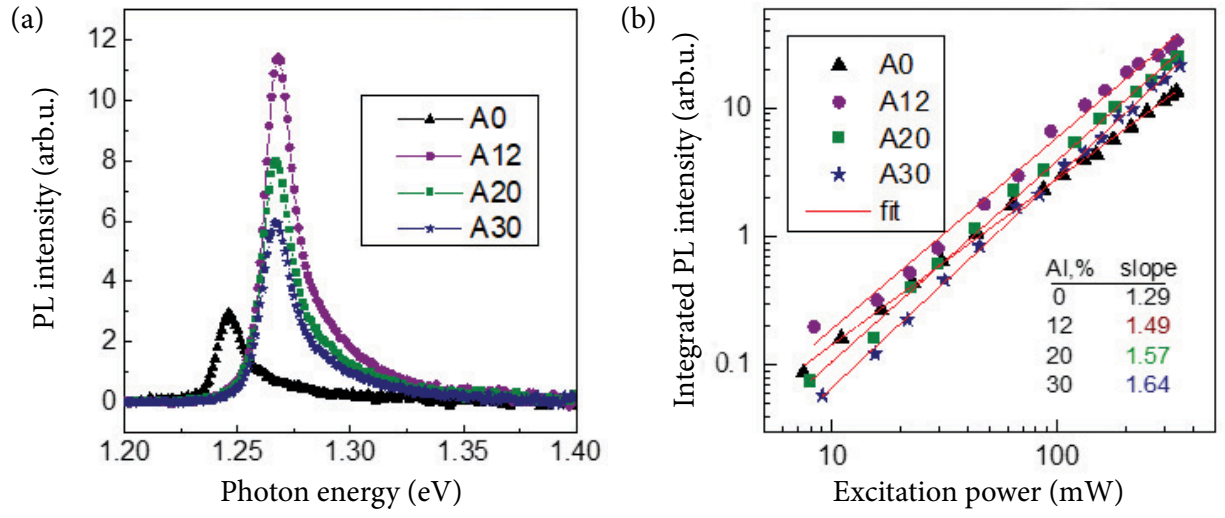


Fig. 3. Room temperature PL measurements of the investigated SQW InGaAs/(Al)GaAs structures. (a) RTPL spectra under excitation of 5 kWcm$^{-2}$. (b) Integrated PL intensity dependence on the excitation power in a double logarithm scale (symbols) and fitting with the power law function (lines).

Table 1. Optical properties for the investigated samples. The RTPL emission of each sample is reported in the first column. In the second column, the emission calculated via nextnano[3] for 20.8% In content. The third column shows the In content obtained by fitting the PL emission using the same simulations.

| Sample | Experimental emission, eV | Calculated emission, eV | Estimated In content, % |
|---|---|---|---|
| A0 | 1.2452 | 1.2609 | 21.5 |
| A12 | 1.2675 | 1.2664 | 20.7 |
| A20 | 1.2674 | 1.2726 | 21.4 |
| A30 | 1.2667 | 1.2787 | 22.0 |

In Table 1, the measured PL emission and the calculated ones are reported.

Three potential explanations are considered for this anomaly. First, the aluminium content calibration during one of the two growths could have been inaccurate, resulting in both samples having the same barrier composition, with an aluminium concentration between 0 and 30%. This possibility can be easily addressed. Due to the lattice matching between GaAs and AlGaAs, the intensity oscillations of the RHEED pattern are well-defined, allowing many oscillations to be visible, and this facilitates precise measurements and an accurate estimation of the Al content in the barriers.

Second, the QW thickness may differ, with the variation in width compensating for the differences in the barrier material. Since InGaAs (bulk) is not lattice-matched to GaAs, the number of observable RHEED intensity oscillations is lower, making the growth rate measurement less reliable. Assuming a measurement error of approximately 1.5%, the QW thickness could vary by the same percentage. For instance, if the InGaAs growth rate was 630 nm/h instead of the nominal 620 nm/h, the QW thickness would be 5.79 nm instead of 5.7 nm. The previous work, including the XRD analysis of grown structures, indicates that MBE growth can achieve highly precise layer thicknesses. However, the samples in this study consist of too few layers for XRD characterization.

Third, the indium content in the QW might differ between the two samples, compensating for the variation in Al content in the barriers. As mentioned earlier, the InGaAs growth rate measurement is less reliable than that of GaAs or AlGaAs. If we apply the same 1.5% deviation considered earlier, the indium content could shift from 20.8 to 22.0%.

To explore these possibilities, simulations were conducted to assess the impact of shifts in the indium content and QW thickness on emission energy. Figure 1 presents the calculated levels in the quantum wells, allowing to calculate emission energies for each sample as a function of both parameters. By fitting the simulated emission energy with the experimental values obtained by RTPL, samples A0 and A20 were likely grown with an indium content of around 21.5%, A12 contained approximately 21%, and A30 had 21.8%.

From the spectra shown in Fig. 3(a), a difference in PL emission intensity appears obvious. To investigate the cause of this difference, further measurements were performed. The surface quality was analyzed using AFM. In Fig. 4, the maps are shown for all samples investigated in this work. The RMS values for the different samples are between 0.8 and 0.9 nm. From these measurements, we can conclude that no difference between the quality surface of the samples is visible via AFM.

Two samples with 12 QWs, with Al 0 and 30% in the barriers, were grown as reference samples and XRD was used to evaluate the interface quality. The $\Omega$–$2\Theta$ scans are presented in Fig. 5. No significant difference in quality could be observed, except for the absence of some fringes that is likely related to different thickness ratios between wells and barriers. This could be explained by changes at the interface initiated by indium segregation.

Room temperature power law measurements and fits are shown in Fig. 3(b). The slope of the fit depends on the type of recombination that is taking place in the QW. In particular, a slope of 1 would mean that radiative recombination is dominating in the sample. From the fit, we can see that the slope moves further away from 1 with the increase in the Al content in the barrier. This means that the increase in the aluminium content leads to the decrease in the quality of the InGaAs layer and to the increase in the number of non-radiative recombination centres. This result is in line with the previously reported results, in which the decrease in emission intensity is attributed to the formation of a quaternary compound, AlInGaAs, at the interface between the first barrier and the QW [22]. Nevertheless, this measurement alone seems to contradict

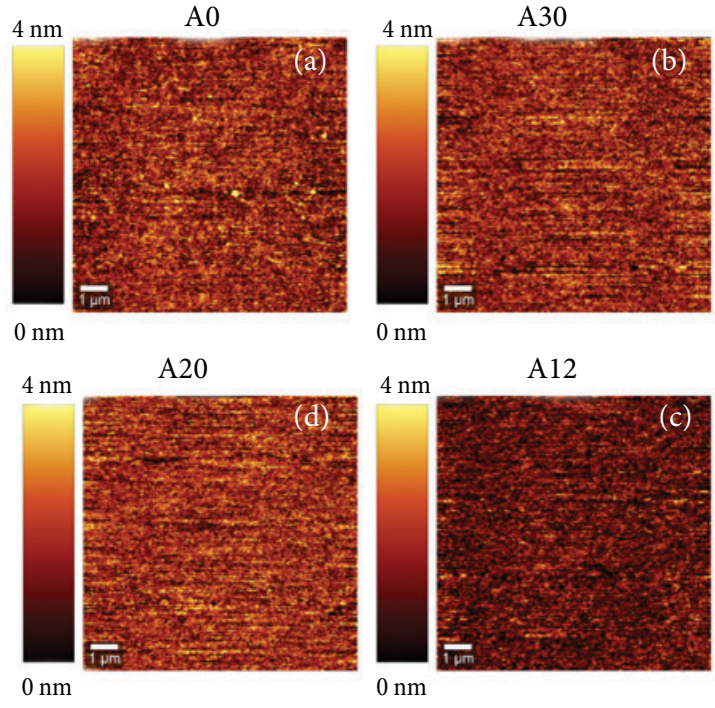


Fig. 4. AFM maps of the presented samples. (a) A0 with RMS($S_q$) = 0.9 nm. (b) A30 with RMS($S_q$) = 0.8 nm. (c) A20 with RMS($S_q$) = 0.9 nm. (d) A12 with RMS($S_q$) = 0.8 nm.

the results of the RTPL, where all samples with AlGaAs barriers show a higher intensity.

TDPL measurements were performed on all samples. In Fig. 6(a), the spectra of sample A12 are shown. In Fig. 6(b), the temperature dependences of the spectral position of PL bands for all investigated structures are given. These data were fitted

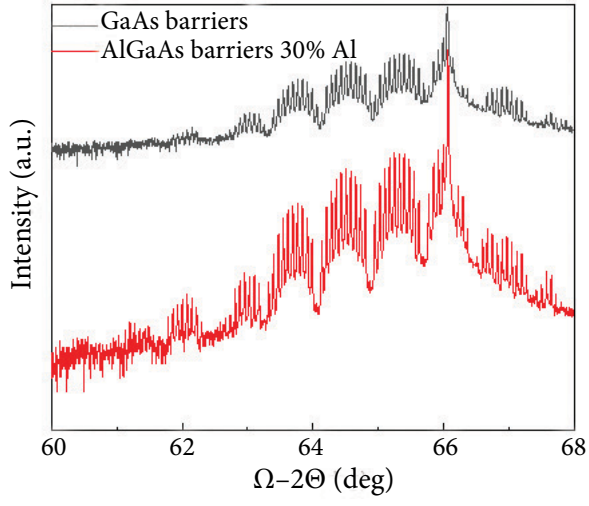


Fig. 5. XRD scans of two reference samples with 12 InGaAs QWs. A black curve rapresents the sample with GaAs barriers, and the measurement of sample with AlGaAs (30% Al) barriers is shown in red.

Table 2. Best fitting parameters of the PL peak position versus the temperature curve using the Varshni equation [24].

| Sample | $E_0$, eV | $\alpha$, meVK$^{-1}$ | $\beta$, K |
|---|---|---|---|
| A0 | 1.332 ± 0.001 | 0.68 ± 0.04 | 428 ± 41 |
| A12 | 1.350 ± 0.001 | 0.65 ± 0.04 | |
| A20 | 1.354 ± 0.001 | 0.66 ± 0.04 | |
| A30 | 1.350 ± 0.001 | 0.67 ± 0.04 | |

using the Varshni equation [24]. The parameters resulting from such fits are shown in Table 2. The temperature dependence of the integrated PL intensity for all samples is shown in Fig. 6(c). We can notice that at low temperature the sample without AlGaAs barriers A0 exhibits the highest PL intensity, as expected from the results obtained from the power law measurements. The PL intensity of A0 starts dropping at around 75 K, and at around 200 K all the examined samples have the same PL intensity. At room temperature, the relation between intensities is the same as one observed in Fig. 3(a), with A0 being the least intense and A12 the most intense.

Combining the results of TDPL and power law measurements, we can conclude that the introduction of Al in the barrier of InGaAs QWs leads to a decreased QW quality and the increase in

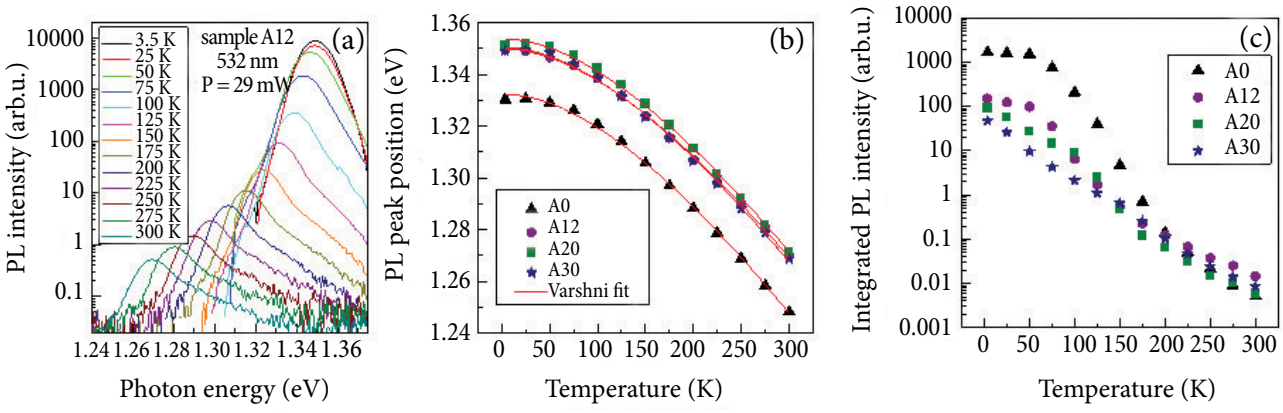


Fig. 6. (a) Temperature-dependent PL spectra of SQW InGaAs/AlGaAs containing 12% of Al in the barrier. (b) Temperature dependences of the spectral position of PL bands for all investigated structures. Symbols correspond to the experimental data, whereas the solid lines are fitted using the Varshni equation [24]. (c) Temperature dependence of the integrated PL intensity for all investigated structures.

non-radiative recombination centres; this can be observed both in the power law measurements and in the low temperature integrated PL intensity of different samples. In particular, the higher the Al content is, the lower the InGaAs quality becomes, at least in the studied range of 0–30%.

Nevertheless, at temperatures higher than 200 K, the integrated PL intensity in the sample A0 drops due to the thermal escape of the carriers, while the presence of Al in the barriers confines the carrier within the QW. Therefore, the highest PL intensity at room temperature is observed in A12, as it has the best structural quality, as follows from the power law measurements, due to the lowest Al content and enough Al in the barrier to avoid the thermal escape of the carriers.

## 4. Conclusions

Four samples, each of them consisting of an InGaAs quantum well with different barrier composition, were modelled and grown. One sample with a GaAs barrier and three of them with AlGaAs barriers contain different aluminium contents, 12, 20 and 30%. Calculations using nextnano[3] were performed to evaluate the band structure of the four samples, and to visualize the levels in the QWs and estimate the real indium content in the QW. The modelled structures were subsequently grown via MBE, on semi-insulating GaAs substrates.

From temperature-dependent photoluminescence, the emission intensity of the samples was compared, and from power law measurements, the quality of the InGaAs layer was estimated. The results of this investigation led to the conclusion that the aluminium content in the barrier reduces the quality of the QW, increasing the number of non-radiative recombination centres, thus decreasing the emission intensity.

At the same time, at high temperature, the presence of Al in the barrier blocks the thermal escape of the carriers from the QW, leading to a higher intensity of the emission at room temperature.

We can conclude that for application in light emitting devices the optimal amount of Al to employ in the barrier of InGaAs QWs is tightly related to the target operation temperature of the device. Balancing these two effects for the samples emitting at NIR, the highest emission intensity at room temperature was achieved in the QW with AlGaAs barriers containing 12% aluminium.

## Acknowledgements

This research has received funding from the Research Council of Lithuania (LMTLT), Agreement No. S-PD-22-7.

## References

[1] S. Hu, D. Young, S. Corzine, A. Gossard, and L. Coldren, High-efficiency and low-threshold InGaAs/AlGaAs quantum-well lasers, J. Appl. Phys. **76**, 3932–3934 (1994).

[2] F. Beffa, H. Jäckel, M. Achtenhagen, C. Harder, and D. Erni, High-temperature optical gain of

980 nm InGaAs/AlGaAs quantum-well lasers, Appl. Phys. Lett. **77**, 2301–2303 (2000).

[3] L. Han, M. Zhao, X. Tang, W. Huo, Z. Deng, Y. Jiang, W. Wang, H. Chen, C. Du, and H. Jia, Luminescence study in InGaAs/AlGaAs multi-quantum-well light emitting diode with p-n junction engineering, J. Appl. Phys. **127**, 085706 (2020).

[4] H. Yang, Y. Zheng, Z. Tang, N. Li, X. Zhou, P. Chen, and J. Wang, MBE growth of high performance very long wavelength InGaAs/GaAs quantum well infrared photodetectors, J. Phys. D **53**, 135110 (2020).

[5] B. Heinen, T.-L. Wang, M. Sparenberg, A. Weber, B. Kunert, J. Hader, S.W. Koch, J.V. Moloney, M. Koch, and W. Stolz, 106 W continuous wave output power from vertical-external-cavity surface-emitting laser, Electron. Lett. **48**(9), 516–517 (2012).

[6] D. Das, H. Ghadi, B. Tongbram, S. Singh, and S. Chakrabarti, The impact of confinement enhancement AlGaAs barrier on the optical and structural properties of InAs/InGaAs/GaAs submonolayer quantum dot heterostructures, J. Lumin. **192**, 277–282 (2017).

[7] H. Dong, J. Sun, S. Ma, J. Liang, T. Lu, Z. Jia, X. Liu, and B. Xu, Effect of potential barrier height on the carrier transport in InGaAs/GaAsP multi-quantum wells and photoelectric properties of laser diode, Phys. Chem. Chem. Phys. **18**, 6901–6912 (2016).

[8] Y.-F. Wang, M.I. Niass, F. Wang, and Y.-H. Liu, Improvement of radiative recombination rate in deep ultraviolet laser diodes with steplike quantum barrier and alluminum content-graded electron blocking layers, Chinese Phys. B **29**, 017301 (2020).

[9] Y. Yazawa, T. Kitatani, J. Minemura, K. Tamura, K. Mochizuki, and T. Warabisako, AlGaAs solar cells grown by MBE for high-efficiency tandem cells, Sol. Energy Mater. Sol. Cells **35**, 39–44 (1994).

[10] K. Chang, J. Wu, D. Liu, D. Liou, and C. Lee, High quality AlGaAs layers grown by molecular beam epitaxy at low temperatures, J. Mater. Sci.: Mater. Electron. **3**, 11–15 (1992).

[11] A. Chin and K. Lee, High quality Al(Ga)As/GaAs/Al(Ga)As quantum wells grown on (111)A GaAs substrates, Appl. Phys. Lett. **68**, 3437–3439 (1996).

[12] W. Liu, Investigation of electrical and photoluminescent properties of MBE-grown $Al_xGa_{1-x}As$ layers, J. Mater. Sci. **25**, 1765–1772 (1990).

[13] S. Miyazawa, Y. Sekiguchi, and M. Okuda, High-reliability GaAs/AlGaAs multiquantum well lasers grown at a low temperature (375°C), Appl. Phys. Lett. **63**, 3583–3585 (1993).

[14] S. Fujimoto, M. Aoki, and Y. Horikoshi, X-ray analysis of In distribution in molecular beam epitaxy grown InGaAs/GaAs quantum well structures, Jpn. J. Appl. Phys. **38**, 1872–1874 (1999).

[15] M. Mashita, Y. Hiyama, K. Arai, B. Koo, and T. Yao, Indium reevaporation during molecular beam epitaxial growth of InGaAs layers on GaAs substrates, Jpn. J. Appl. Phys. **39**, 4435 (2000).

[16] K. Muraki, S. Fukatsu, Y. Shiraki, and R. Ito, Surface segregation of In atoms during molecular beam epitaxy and its influence on the energy levels in InGaAs/GaAs quantum wells, Appl. Phys. Lett. **61**, 557–559 (1992).

[17] L.C. Andreani, A. Pasquarello, and F. Bassani, Hole subbands in strained GaAs-GaAlAs quantum wells: Exact solution of the effective mass equation, Phys. Rev. B **36**, 5887 (1987)

[18] Y. Maidaniuk, R. Kumar, Y.I. Mazur, A. Kuchuk, M. Benamara, P. Lytvyn, and G. Salamo, Indium segregation in ultra-thin In(Ga)As/GaAs single quantum wells revealed by photoluminescence spectroscopy, Appl. Phys. Lett. **118**, 062104 (2021).

[19] W. Liu, H. Wang, J. Wang, Q. Wang, J. Wang, J. Fan, Y. Zou, and X. Ma, The improvement properties of InGaAs/InGaAsP multiple quantum wells using the GaAs insertion layer, Thin Solid Films **756**, 139363 (2022).

[20] M. Hino, M. Asami, K. Watanabe, Y. Nakano, and M. Sugiyama, Enhanced radiative efficiency of InGaAs/GaAsP multiple quantum wells by optimizing the thickness of interlayers, Phys. Status Solidi A **219**, 2100426 (2022).

[21] B. Zhang, H. Wang, X. Wang, Q. Wang, J. Fan, Y. Zou, and X. Ma, Effect of GaAs insertion layer

on the properties improvement of InGaAs/AlGaAs multiple quantum wells grown by metal-organic chemical vapor deposition, J. Alloys Compd. **872**, 159470 (2021).

[22] Z. Yang, B. Qiu, S. Ma, B. Xu, Y. Shi, S. Yuan, L. Shang, X. Hao, and J. Zhang, InGaAs/AlGaAs MQWs grown by MBE: Optimizing GaAs insertion layer thickness to enhance interface quality and luminescent property, Mater. Sci. Semiconduct. Process. **180**, 108584 (2024).

[23] A. Zelioli, A. Špokas, B. Čechavičius, M. Talaikis, S. Stanionytė, A. Vaitkevičius, A. Čerškus, E. Dudutienė, and R. Butkutė, In-depth investigation of emission homogeneity of InGaAs multiple quantum wells using spatially resolved spectroscopy. Available at SSRN: https://ssrn.com/abstract=4813221 or http://doi.org/10.2139/ssrn.4813221 (2024).

[24] Y.P. Varshni, Temperature dependence of the energy gap in semiconductors, Physica **34**(1), 149–154 (1967).

## AlGaAs BARJERO OPTIMIZAVIMAS InGaAs KVANTINĖMS DUOBĖMS, SPINDULIUOJANČIOMS ARTIMOJOJE INFRARAUDONOJOJE SPEKTRO SRITYJE

A. Zelioli [a], J. Žuvelis [a, b], U. Cibulskaitė [b], A. Špokas [a, b], E. Dudutienė [a], A. Vaitkevičius [a, b], S. Stanionytė [a], B. Čechavičius [a], R. Butkutė [a]

[a] *Valstybinis mokslinių tyrimų institutas Fizinių ir technologijos mokslų centras, Vilnius, Lietuva*

[b] *Vilniaus universiteto Fotonikos ir nanotechnologijų institutas, Vilnius, Lietuva*

**Santrauka**

Tirta pavienių InGaAs kvantinių duobių darinių optinės kokybės priklausomybė nuo barjero dizaino. Dariniai su viena stačiakampe InGaAs kvantine duobe (~21 % indžio) ir AlGaAs barjerais (su skirtingomis Al koncentracijomis nuo 0 iki 30 %) buvo modeliuojami nextnano³ programine įranga, siekiant įvertinti sugerties juostos kraštą ir lygmenis kvantinėje duobėje. Serija bandinių buvo užauginta ant pusiau izoliuojančių GaAs padėklų naudojant molekulinių pluoštelių epitaksiją. Atominių jėgų mikroskopija ir rentgeno spindulių difrakcija buvo naudojamos bandinių paviršių šiurkštumui ir sluoksnių sąlyčio ribų kokybei įvertinti. Fotoliuminescencijos tyrimai suteikė informacijos apie Al koncentracijos AlGaAs barjere įtaką kvantinių duobių optinei kokybei bei krūvininkų sąspraudai. Tyrimai atskleidė, kad didėjant Al koncentracijai AlGaAs barjere padidėja krūvininkų pagavimas kvantinėje duobėje, bet kartu prastėja InGaAs kvantinės duobės kristalografinė kokybė. Buvo nustatyta, kad barjeras su 12 % Al gali būti naudojamas šiems efektams subalansuoti, pasiekiant optimalią krūvininkų sąspraudą, bei išlaikant patenkinamą kvantinės duobės kristalinę kokybę.